J Biol Phys (2012) 38:153–168
DOI 10.1007/s10867-011-9246-4

ORIGINAL PAPER

Conformational changes in the archaerhodopsin-3 proton pump: detection of conserved strongly hydrogen bonded water networks

Erica C. Saint Clair · John I. Ogren · Sergey Mamaev · Joel M. Kralj · Kenneth J. Rothschild

Received: 15 October 2011 / Accepted: 25 October 2011 /
Published online: 10 December 2011

Abstract Archaerhodopsin-3 (AR3) is a light-driven proton pump from *Halorubrum sodomense*, but little is known about its photocycle. Recent interest has focused on AR3 because of its ability to serve both as a high-performance, genetically-targetable optical silencer of neuronal activity and as a membrane voltage sensor. We examined light-activated structural changes of the protein, retinal chromophore, and internal water molecules during the photocycle of AR3. Low-temperature and rapid-scan time-resolved FTIR-difference spectroscopy revealed that conformational changes during formation of the K, M, and N photocycle intermediates are similar, although not identical, to bacteriorhodopsin (BR). Positive/negative bands in the region above 3,600 cm^{-1}, which have previously been assigned to structural changes of weakly hydrogen bonded internal water molecules, were substantially different between AR3 and BR. This included the absence of positive bands recently associated with a chain of proton transporting water molecules in the cytoplasmic channel and a weakly hydrogen bonded water (W401), which is part of a hydrogen-bonded pentagonal cluster located near the retinal Schiff base. However, many of the broad IR continuum absorption changes below 3,000 cm^{-1} assigned to networks of water molecules involved in proton transport through cytoplasmic and extracellular portions in BR were very similar in AR3. This work and subsequent studies comparing BR and AR3

This work was supported by National Institutes of Health Grants R01GM069969 and R01 EY021022 to KJR.

E. C. Saint Clair · J. I. Ogren · S. Mamaev · K. J. Rothschild
Department of Physics, Photonics Center and Molecular Biophysics Laboratory,
Boston University, Boston, MA 02215, USA

J. M. Kralj
Chemistry and Chemical Biology, Harvard University, Cambridge, MA 02138, USA

K. J. Rothschild (✉)
Department of Physics, Boston University, 590 Commonwealth Avenue, Boston, MA 02215, USA
e-mail: kjr@bu.edu

structural changes will help identify conserved elements in BR-like proton pumps as well as bioengineer AR3 to optimize neural silencing and voltage sensing.

Keywords Archaerhodopsin-3 · Bacteriorhodopsin · FTIR difference spectroscopy · Proton pump · Membrane protein · Water networks · Protein conformational changes · Biomembranes · Energy transduction

Abbreviations

AR3	Archaerhodopsin-3
BR	Bacteriorhodopsin
FTIR	Fourier transform infrared
OG	Octylglucoside
RRS	Resonance Raman spectroscopy
ECPL	*E. coli* polar lipids
RSB	Retinal Schiff base

1 Introduction

Bacteriorhodopsin (BR), a member of the archaeal rhodopsin family [1] found in *Halobacterium salinarum*, is one of the most extensively studied membrane proteins. It serves as a model for many other ion transport, sensory, and energy-transducing membrane proteins involved in key cellular processes [2, 3]. While a general model of BR light-driven proton pumping has emerged on the basis of over four decades of spectroscopic studies such as FTIR-difference spectroscopy [4, 5] and X-ray crystallography [3, 5], key questions still remain about important details of the proton pump mechanism including the role of internal water molecules [6, 7].

Structural changes in internal waters during the BR photocycle were first detected by low-temperature FTIR-difference spectroscopy [7–9]. The earliest changes occur during the primary phototransition ($BR_{570} \rightarrow K_{630}$) and involve weakly hydrogen bonded waters as evidenced by an OH (hydroxyl) stretch vibration detected at 3,642 cm^{-1}, which downshifts by 12 cm^{-1} in H_2O^{18}. Such hydroxyls are often termed "dangling" because the OH stretching mode is upshifted several hundred wavenumbers from the frequency of the more fully hydrogen-bonded hydroxyl groups found in bulk water. Dangling hydrogen bonds are also found in water confined to small volumes such as in the interior of a protein or a single chain of water in a carbon nanotube where the normal hydrogen bonds found in bulk water cannot be established [10].

Since the OH stretching frequency of the hydroxyl groups in water is expected to be extremely sensitive to changes of local environment [11, 12], it can be used to provide information about the structure and dynamics of these internal waters during the photocycle. Furthermore, comparison of the protonation and hydrogen bonding changes of internal water molecules across microbial rhodopsin species will reveal information about functionally conserved mechanisms involving internal waters.

In this work, archaerhodopsin-3 (AR3), a light-driven proton pump found in *Halorubrum sodomense*, is studied for the first time using FTIR-difference spectroscopy. AR3 is closely related to archaerhodopsin-1 (AR1) and archaerhodopsin-2 (AR2) with over 90% homology [1]; the structures of AR1 and AR2 have previously been solved by X-ray crystallography [13]. AR3 is also closely related to BR, with over 75% sequence homology.

Significantly, all key residues implicated in proton pumping in BR are conserved, including the transmembrane Asp and Glu residues (see Fig. 1 of reference [1]). However, little is known about the detailed proton pump mechanism of AR3 or the closely related species AR1 and AR2 (see [1]). FTIR-difference spectroscopy provides the ability to compare light-driven structural changes in BR and AR3 at the level of individual molecular groups during the photocycle, especially in the OH stretch region, which reflects internal water molecules.

Motivation for studying AR3 also derives from the recent discovery that it can serve both as a high-performance genetically-targetable optical neural silencer [14] and as a fluorescent sensor of transmembrane potential [15]. Understanding the structural basis for how AR3 functions will provide critical information for intelligently engineering this protein and other microbial rhodopsins to optimize their performance as photonic components in the rapidly evolving field of optogenetics [16].

Our results indicate that AR3 and BR undergo similar structural changes during their photocycles, including similar protonation/deprotonation of key Asp residues. However, we also find evidence for a possible difference in the Schiff base reprotonation mechanism. In addition, there are differences in the water region above 3,600 cm^{-1} previously assigned in BR to weakly hydrogen bonded internal water molecules located in the cytoplasmic channel and near the BR retinal Schiff base. Most striking are the conservation of broad continuum IR absorbance changes in BR and AR3 that have previously been associated in BR with networks of strongly hydrogen-bonded water molecules involved in proton transport [17–19].

2 Materials and methods

2.1 Protein expression and purification

A lentiviral backbone plasmid encoding Arch-EGFP (FCK: Arch-EGFP) was a generous gift from Dr. Edward Boyden (MIT). Although the codon usage had been optimized for expression in mammalian neurons, it did not prevent expression in *E. coli* (see below). The gene for AR3 was cloned into pet28b vector (EMD Biosciences) using the restriction sites EcoRI and NcoI keeping the Histag in frame. Proper insertion was checked by sequencing. AR3 was expressed and purified from *E. coli*, similar to published procedures [20]. Briefly, *E. coli* (strain BL21, pet28b plasmid) was grown in 1 L of LB with 100 mg/ml kanamycin, to an O.D. of 0.4 at 600 nm at 37°C. All-*trans* retinal (5 mM) and inducer (IPTG 0.5 mM) were added and cells were grown for an additional 3.5 h in the dark at 32°C. Cells were then harvested by centrifugation and resuspended in sonication buffer (50 mM Tris, 2 mM $MgCl_2$ at pH 7.3) and lysed with a tip sonicator for 5 min, three times on ice. The lysate was centrifuged and the pellet was resuspended in binding buffer (50 mM K_2HPO_4, 300 mM NaCl 1.5% octylglucoside (OG) and 5 mM imidazole at pH 7.0). The mixture was homogenized with a glass/Teflon Potter Elvehjem homogenizer and centrifuged again. Ni-NTA Agarose (QIAGEN) beads were added to the supernatant, washed with binding buffer and incubated 1 h at 4°C using a rotary shaker. Ni-NTA agarose beads with bound AR3 were loaded into a 3-ml disposable plastic column and washed with 2 ml of binding buffer. AR3 was eluted with 1 ml of elution buffer (50 mM K_2HPO_4, 300 mM NaCl, 1.5% OG and 250 mM imidazole at pH 7.0). Purified His-tagged AR3 was reconstituted in *E. coli* polar lipids (ECPL) (Avanti, Alabaster, AL) at 1:10 protein-to-lipid (w/w) ratio. Lipids initially dissolved in chloroform were dried under argon and resuspended in dialysis buffer (50 mM

K_2HPO_4, 300 mM NaCl) to which OG was added to the final concentration of 1%. The lipid solution was incubated with the OG-solubilized protein for 1 h on ice and dialyzed against the dialysis buffer overnight at 4°C, followed by buffer change and an additional dialysis of 3 h. The reconstituted protein was centrifuged for 10 min and resuspended in dialysis buffer three times. AR3 samples were stored at 4°C. Typical yields based on measurement of the OD at 570 nm for the reconstituted AR3 proteoliposomes ranged from 400 μg up to 800 μg per liter of *E. coli* culture.

3 FTIR difference spectroscopy

The protein samples for the low-temperature FTIR measurements were prepared as previously reported [20, 21] using approximately 200 μg of the protein for each experiment. The samples were deposited on CaF_2 windows and dried under a slow stream of argon. Samples were then rehydrated via the vapor phase and sealed in a sample cell with another CaF_2 window and mounted on a liquid nitrogen cryostat (ARS Cryo Helitran LT-3). Low-temperature FTIR difference spectra were recorded using a protocol similar to that reported previously on green proteorhodopsin [21–23], BR [24, 25], and other microbial rhodopsins [26, 27]. For measurements at 80 K, the samples were first cooled in the dark from a light-adapted state at room temperature to avoid trapping of photointermediates. After thermal stabilization the sample was illuminated with blue light ($415 < \lambda < 500$ nm) for 5 min after which a spectrum of 1,000 scans was recorded at 4 cm^{-1} using a Bio-Rad FTS-60A FTIR spectrometer (Bio-Rad, Digilab Division, Cambridge, MA) equipped with a liquid nitrogen cooled HgCdTe detector. The sample was then illuminated with long-wavelength orange light ($800 \text{ nm} > \lambda > 570$ nm) for 5 min; a second spectrum was recorded in the dark and subtracted from the first. At least 20 such cycles of blue and orange light were repeated and the difference spectra averaged in order to increase the signal-to-noise ratio. In addition, all experiments were performed with at least two independent samples. A Dolan-Jenner (Woburn, MA) model 180 illuminator (150 W, tungsten-halogen) and a fiber-optic light guide were used for sample illumination in combination with 500-nm low-pass and 570-nm long-pass optical filters (Corion Corp., Holliston, MA).

Spectra at 230, 240, and 250 K were taken using procedures similar to those previously reported for BR [28] at 250 K. Differences were computed by subtracting spectra of AR3 recorded in the dark from a spectrum recorded at the same temperature while illuminating the sample with yellow light (550-nm broad-band interference filter, Ditric Optics, Hudson, MA). This "off/yellow" illumination sequence was repeated up to 50 times, and the successive differences were averaged together. By examining the 5-min dark scans obtained after illumination, it was found at 230–250 K that thermal decay of the M or N intermediate back to AR3 570 nm state was complete within 5 min.

3.1 Rapid scan time-resolved measurements

Protein films were prepared by depositing 50–100 μl of the proteoliposome suspension in a buffer consisting of 10 mM NaCl and 5 mM NaH_2PO_4 adjusted to pH 7.5 onto a polished 1-mm-thick, 25-mm-diameter CaF_2 window (Crystran, Poole, UK) and drying the sample under a gentle stream of argon. Films were rehydrated via the vapor phase and then sealed in a temperature-controlled IR cell (Model TFC, Harrick Scientific Corp., Ossining, NY) using a second CaF_2 window. Rapid scan time-resolved FTIR spectra were recorded with a Bruker

IFS 66 v/s FTIR spectrometer (Bruker Optics, Germany) at 5°C as described previously [29] with 4 cm^{-1} spectral resolution and 320-kHz scanner velocity corresponding to the data acquisition window of 18 ms. Data blocks of 500 scans were taken, each containing 80 time-resolved difference spectra. Between 10 and 20 individual data blocks were averaged to produce the final spectrum.

4 Results

4.1 Primary phototransition of AR3 involves all-*trans* to 13-*cis* chromophore isomerization

The FTIR difference spectrum of the AR3→K transition (K spectrum minus light-adapted AR3) recorded at 80 K (Fig. 1) showed that, like BR and all other archaeal rhodopsins studied, the initial photochemistry involved all-*trans* to 13-*cis* isomerization of the retinylidene chromophore (see for example recent FTIR studies on green and blue proteorhodopsin [30]). In agreement, resonance Raman (RRS) measurements using 785-nm near-infrared excitation revealed that the AR3 chromophore has an all-*trans* structure very similar to BR (manuscript in preparation, E.C. Saint Clair, J.I. Ogren and K.J. Rothschild).

The overall difference spectrum of AR3→K was very similar to the difference spectrum of BR→K [24, 25, 31, 32] recorded under identical conditions. In the ethylenic stretching region, negative/positive bands appeared at 1,530 (−) and 1,520 (+) cm^{-1}, which are assigned to the ethylenic C=C stretching modes of the retinal chromophore for the initial and K photointermediate, respectively. The negative ethylenic band in AR3 was at a slightly higher frequency than that of BR (1,530 vs. 1,529 cm^{-1}), which is in agreement with

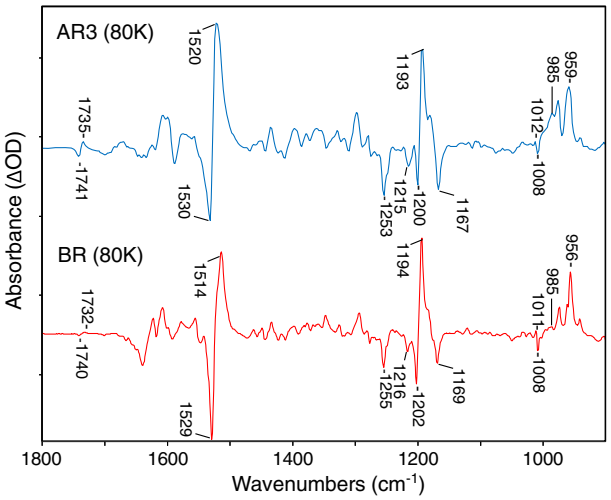

Fig. 1 Comparison of FTIR difference spectra recorded at 4 cm^{-1} spectral resolution for AR3 and BR (*bottom*) at 80 K in the 900–1,800 cm^{-1} region. Each spectrum represents the average of at least 20 difference spectra, each consisting of 1,000 individual scans. Spacing of Y-axis (difference absorbance) markers corresponds to 10 mOD for the BR trace and 0.5 mOD for the AR3 trace. Spectra were scaled by the negative 1,200 C–C retinal stretch band. For lighting sequence used to obtain difference spectrum, see Section 3. Only the frequency of bands discussed in this paper are labeled in this and subsequent figures

a slight upshift measured by resonance Raman spectroscopy (RRS data not shown). An empirical inverse relationship between the visible absorption maximum and the ethylenic stretching frequency has been established for rhodopsins [33] and microbial rhodopsins (see for example [21, 26, 34]), which indicates that such an upshift might correspond to a few nanometer blue-shift of the λ_{max} of AR3 relative to BR at 80 K. The λ_{max} of light-adapted AR3 reconstituted in *E. coli* polar lipids at room temperature was found to be near 570 nm (data not shown) but the UV-visible absorption at 80 K has not yet been measured.

In addition, the positive ethylenic band at 1,520 cm^{-1} from the K intermediate of AR3 at 80 K, was 6 cm^{-1}, higher than for BR. This indicates that the K intermediate may be blue shifted by as much as 30 nm. One possibility is that the AR3 chromophore relaxes at 80 K into a higher temperature form. At 135 K, the positive band in BR has such an upshift in ethylenic stretching frequency (see for example [35]). It has been shown previously using FTIR difference spectroscopy that the K intermediate consists of a number of conformational substates [36], which may differ for AR3 and BR at 80 K.

Prominent negative bands were found in the AR3 retinal fingerprint region at 1,253, 1,215, 1,200, and 1,167 cm^{-1} close to peaks at 1,255, 1,216, 1,202, and 1,169 cm^{-1} appearing in BR and assigned to an all-*trans* retinal chromophore configuration (Fig. 1) [32]. These bands were also found in the RRS of AR3 and thus can be assigned unambiguously to retinal vibrations. A major positive band appeared in the AR3 fingerprint region at 1,193 cm^{-1} close to the 1,194 cm^{-1} band in BR assigned to the mixed stretching vibration of the 13-*cis* retinal chromophore [37]. Overall, the similarity of the fingerprint region for AR3 and BR firmly establishes that the chromophore undergoes an all-*trans* to a 13-*cis* isomerization as previously established for BR on the basis of RRS studies of isotopic labeled retinal in BR [37, 38].

AR3 also exhibited a pair of bands at 1,012/1,008 (+/−) cm^{-1}, assigned to the methyl rock vibrations of the retinal chromophore in BR at similar frequencies [21, 39, 40]. In the hydrogen out-of-plane mode region (900–1,000 cm^{-1}), positive bands appeared in the AR3→ K difference spectrum at 985 and 959 cm^{-1} close to frequencies measured in BR. The intensification of the 985 cm^{-1} band relative to BR is again consistent with stabilization of a higher temperature K-intermediate form in AR3 compared to BR [35].

A pair of negative/positive bands appeared at 1,741/1,735 cm^{-1} most likely arising from changes of Asp125, which is homologous to Asp115 in BR. A very similar pair of peaks were detected in the BR→K and assigned to the COOH carboxylic stretch mode of Asp115 [41]. Although definitive assignment of these bands will require further studies using AR3 mutants, these results confirm that very similar protein conformational changes occur during the primary transition in BR and AR3.

4.2 Similar conformational changes occur during M and N intermediates of AR3 and BR

The BR→M and BR→N FTIR-difference spectra of BR exhibit characteristic bands associated with the M and N photointermediates that have been assigned to specific protein residues on the basis of site-directed mutagenesis and isotope labeling [42–44]. We measured the AR3→M and AR3→N spectra and compared them to the corresponding BR difference spectra (Fig. 2). The static, low-temperature FTIR-difference spectra for AR3→M and AR3→N were similar to the corresponding BR difference spectra including all of the alterations characteristic of the transition from M to N in BR. Note, however, that since AR3 appears to build up relatively larger amounts of the N intermediate at 250 K

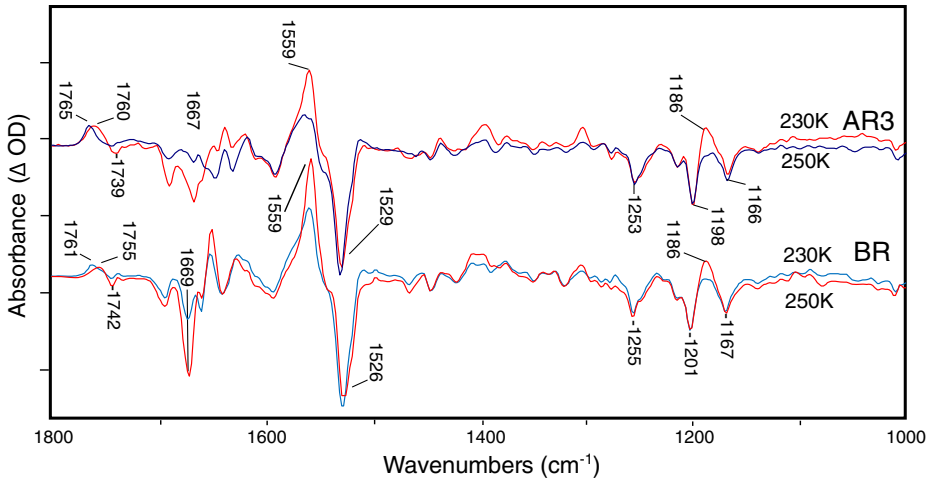

Fig. 2 FTIR difference spectra recorded at 4 cm^{-1} resolution and 230 K (*blue*) and 250 K (*red*) for AR3 and BR at pH 9 in H_2O. Each spectrum represents the average of at least 20 difference spectra, with each spectrum being the average of 1,000 individual scans. Spacing of Y-axis (difference absorbance) markers correspond to 10 mOD for BR at 230 K, 1.5 mOD for BR at 250 K, 0.5 mOD for AR3 at 230 K, and 0.2 mOD for AR3 at 250 K. For lighting sequence used to obtain difference spectrum, see Section 3

compared to BR, we measured BR at pH 9. This has the effect of producing predominantly the N intermediate at 250 K whereas at pH 7 BR accumulates predominantly the M intermediate [45].

In the carboxyl region of the M intermediate spectra (Fig. 2, blue traces) positive bands at 1,761 cm^{-1} (BR) and 1,765 cm^{-1} (AR3) were assigned to the carboxylic acid C=O stretching mode of Asp85. It arises during formation of the M intermediate due to the transfer of a proton from the BR protonated retinal Schiff base to the Asp85 carboxylate group [41]. In contrast, the N difference spectra (Fig. 2, red traces) exhibited a downshift of this band to 1,755 cm^{-1} (BR) and 1,760 cm^{-1} (AR3) and also the appearance of a negative band at 1,739 cm^{-1} (AR3) [42–44], and 1,742 cm^{-1} (BR). The negative band arises from the deprotonation of Asp96, which results in transfer of a proton to the unprotonated retinal Schiff base [46]. The downshift of the 1,760 cm^{-1} band reflects a change in environment of the protonated Asp85 from M to N.

Additional changes between the M and N difference spectra common to both B and AR3 in Fig. 2 include: (i) the appearance of a positive band at 1,186 cm^{-1}, which reflects an increase in intensity of the C-C stretch mode of the 13-*cis* retinylidene chromophore due to protonation of the Schiff base (note that M chromophore also has a 13-*cis* configuration, but the IR intensity of most retinal vibrations are weak due to a deprotonated SB); (ii) increase in a band at 1,555 cm^{-1} reflecting the ethylenic mode of the N-chromophore and the amide II mode; (iii) a negative band at 1,669 cm^{-1} due to changes most likely in the conformation of the α-helical protein structure.

There were also small differences comparing the BR to AR3 spectra in the frequency of several bands in the corresponding M and N difference spectra, potentially reflecting changes in the environment of these groups in BR and AR3. For example, the amide I frequency is upshifted from 1,667 to 1,669 cm^{-1}, indicating slightly weaker α-helix hydrogen bonding in the region of the AR3 structure undergoing a structural change. In

addition, there was an approximate 5-cm^{-1} upshift in frequency of the bands assigned to Asp95 (Asp85 in BR). One possibility is that these small shifts reflect the different lipid environment of BR incorporated into purple membrane patches, which contain specific halobacterial lipids [47] compared to the *E. coli* polar lipids used to reconstitute AR3 for these studies.

We also find that in AR3 that the negative band at 1,739 cm^{-1} had a broader bandwidth and was downshifted several wavenumbers compared to BR. This could arise due to a second Asp or Glu group, which also undergoes a deprotonation in addition to Asp106 and produces a second negative band in this region. In general, this may indicate that the Schiff base reprotonation mechanism in AR3 differs from that in BR. Studies are currently underway using AR3 mutants to confirm and assign this extra band.

4.3 Structural changes of weakly hydrogen bonded internal water in AR3

We found significant differences in bands assigned to weakly hydrogen-bonded internal water molecules in BR and AR3 above 3,600 cm^{-1} (note that the OH stretching mode of water that is weakly hydrogen bonded is normally found in the region from 3,450–3,700 cm^{-1} [48]). In the case of BR, bands appeared during the primary BR→K photoreaction, which were detected at low temperature (80 K) where K decay is blocked [7, 49]. As seen in Fig. 3, negative/positive bands appeared at 3,642/3,636 cm^{-1}, which downshifted approximately 10–13 cm^{-1} when H_2O^{18} is substituted for H_2O [49]. A second positive band at 3,625 cm^{-1} was also assigned to water [49].

In the AR3→K spectrum, a similar positive/negative feature was detected at 80 K (Fig. 3). These spectra were scaled to the BR spectrum using the negative retinal C-C stretch band near 1,200 cm^{-1} to assure that the relative intensity of the water bands reflected approximately the same number of molecules undergoing a photoconversion to K. While the spectral pattern was similar in this region to BR, the negative peak in AR3 was upshifted almost 15 cm^{-1} to 3,657 cm^{-1}, reflecting an even weaker hydrogen bonding of an internal

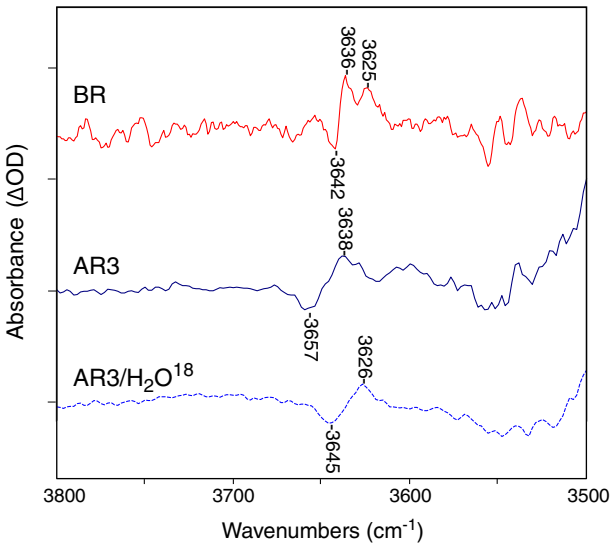

Fig. 3 FTIR difference spectra recorded at 80 K with 4 cm^{-1} resolution (same as Fig. 1 above) for BR (*red*), AR3 (*blue solid*), and AR3/H_2O^{18} (*blue dashed*) in the 3,800–3,500 cm^{-1} region. Each spectrum represents the average of at least 18 difference spectra, with each spectrum being the average of 1,000 individual scans. Spacing of Y-axis (difference absorbance) markers corresponds to 0.06 mOD for the AR3 spectra and 0.1 mOD for the BR spectra. For lighting sequence used to obtain difference spectrum, see Section 3

water hydroxyl group. However, the positive band at 3,638 cm^{-1} appeared close to the same frequency as BR, indicating that it has a similar hydrogen bonding environment in the K intermediate. As in the case of BR, these bands were definitively assigned to an internal water molecule(s) on the basis of the approximately 12 cm^{-1} downshift upon H_2O^{18} substitution (Fig. 3, lower dashed trace).

A much larger difference between AR3 and BR was found in the water region upon formation of M and N intermediates (Fig. 4). As reported previously for BR [49], two positive bands appeared at 3,671 and 3,655 cm^{-1} in addition to a negative band at 3,642 cm^{-1}. In contrast, no such positive bands were detected above 3,600 cm^{-1} in the case of AR3 at 230 and 240 K. Note that at the higher temperature a mixture of M and N appears in AR3 based on bands below 1,800 cm^{-1}. Furthermore, only a small broad negative band that may resolve into two individual bands near 3,655 and 3,642 cm^{-1} appeared, which is weaker relative to the BR band at 3,642 cm^{-1}.

In order to confirm the absence of positive bands in AR3 above 3,600 cm^{-1}, we measured time-resolved FTIR differences at 5°C using the rapid scan technique for both AR3 and BR. Figure 5 shows the results for an average over the first 40 ms after laser excitation where the M intermediate is predominantly present (e.g., BR→M) as based on spectral features discussed previously (blue traces). An average is also shown of later time slices (60 to 100 ms) where M has decayed and the spectrum reflects predominantly the BR→N differences (red trace).

In the case of BR (lower traces, Fig. 5), the bands at 3,670 and 3,656 cm^{-1} and the negative band at 3,642 cm^{-1} were clearly detected for BR→M. Note that the positive 3,670 cm^{-1} band disappeared in the BR→N with only the negative/positive feature at 3,642 and 3,655 cm^{-1}, remaining in agreement with recent time-resolved FTIR studies [17]. This indicates that the 3,670 cm^{-1} positive band is associated predominantly with M and most likely originates from a different water molecule than those giving rise to the 3,642 and 3,655 cm^{-1} bands. In contrast, bands of similar intensity were not seen in this region in the AR3 time-resolved FTIR for both H_2O and H_2O^{18}, in complete agreement with results obtained at lower temperature.

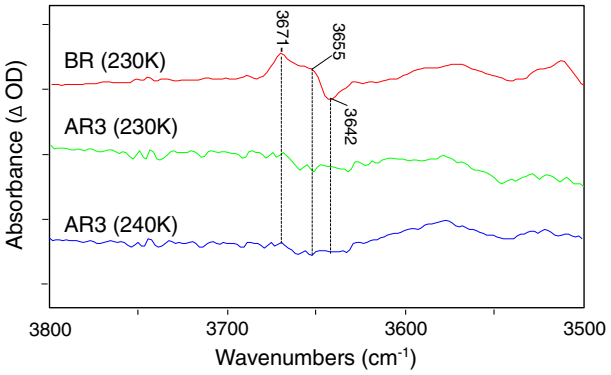

Fig. 4 FTIR difference spectra recorded at 4 cm^{-1} resolution for BR (*red*) at 230 K, AR3 (*green*) at 230 K and AR3 (*blue*) at 240 K in the 3,800–3,500 cm^{-1} region. Each spectrum represents the average of at least 18 difference spectra, with each spectrum being the average of 1,000 individual scans. Spacing of Y-axis (difference absorbance) markers is 2.5 mOD for BR, and 0.15 mOD for AR3 at 230 and 240K. Note that in the AR3 difference spectrum recorded at 240 K corresponds to a mixture of the M and N intermediates. For lighting sequence used to obtain difference spectrum, see Section 3

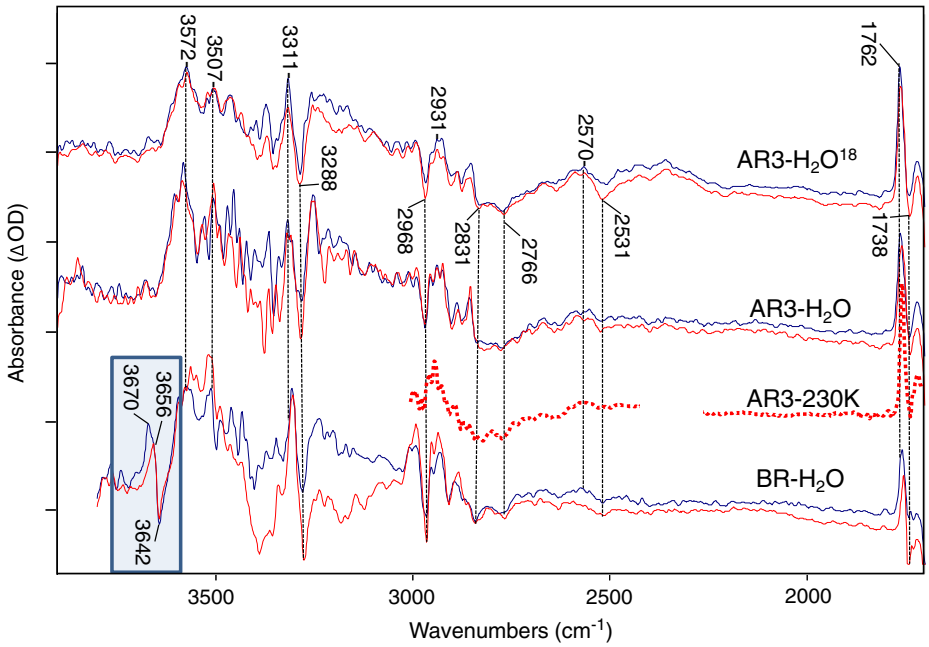

Fig. 5 Time-resolved difference spectra for AR3 WT in H_2O, AR3 WT, in H_2O^{18}, and BR WT in H_2O over the spectroscopic region from 1,700 to 4,000 cm^{-1}. AR3 H_2O and H_2O^{18} data were recorded at neutral pH. BR WT H_2O data was recorded at pH 9. All data was recorded in rapid scan mode on Bruker ifs/v66 model FTIR spectrometer at 4 cm^{-1} resolution, and 320-kHz scanner velocity (see Section 3). Laser luminosity was less than 6 mJ/cm^2 at the sample with repetition rate less than 0.5 Hz to prevent sample burnout. *Blue traces* represent the early averages (zero to 40 ms after the laser excitation) where the sample is predominantly in the M state as evidenced by the 1,762 cm^{-1} bands. The *red traces* represent later averages (60 ms to several hundred ms) where the M state has decayed sufficiently into the N photointermediate. These photointermediate assignments are supported by the intensity of the 1,180 cm^{-1} bands (not shown). Spacing of the Y-axis (difference absorbance) markers corresponds to 0.1 mOD for AR3 H_2O M as well as AR3 H_2O^{18} M and N; 0.05 mOD for AR3 H_2O N and BR H_2O M; and 0.025 mOD for AR3 230K and BR H_2O N spectra. *Dotted line* shows low-temperature spectrum of AR3 at 230K below 3,000 cm^{-1} (see Figs. 2 and 4 captions for more detail). Spectral region obscured by $C0_2$ absorbance band between 2,250 and 2,350 cm^{-1} is not shown

4.4 Similarity of broad IR continuum absorbance in AR3 and BR

Although the bands associated in BR with one or more "dangling" hydrogen bonds above 3,600 cm^{-1} were absent in AR3, there was still a striking similarity for bands below 3,500 cm^{-1} extending to 1,800 cm^{-1} (Fig. 5). For example, there were many negative/positive bands that closely matched, including prominent positive bands at 3,572, 3,507, 3,311, 2,931, and 2,570 cm^{-1} and negative bands at 3,288, 2,968, 2,766, and 2,531 cm^{-1} (see dashed lines in Fig. 5) as well as a number of much smaller bands (unlabeled). Potential chemical groups that could produce such bands include the stretching vibration of OH groups (Ser, Thr, Tyr), NH groups (Trp) and SH groups (Cys).

Only a few bands in this region have been previously assigned in BR and arise from X-H type vibrations. For example, the L intermediate in BR gives rise to an NH stretch mode in the tryptophan indole group at 3,477 cm^{-1} [50]. A positive band near 3,511 cm^{-1} and smaller features at 3,496 cm^{-1} (−) were assigned in the BR→M difference spectrum to a

threonine residue (OH stretch) on the basis of [3–^{18}O]Thr labeling, while a much smaller band appearing at 3,486 cm^{-1} was tentatively assigned to a tryptophan [51] (NH stretch). The appearance of bands at the same position in AR3 indicated that similar residues undergo similar structural changes in AR3.

The similarity between BR and AR3 in this region was especially striking for broad IR continuum absorbance changes below 3,000 cm^{-1} previously assigned to networks of strongly hydrogen bonded waters (see discussion below). A broad positive absorbance centered at 2,570 cm^{-1} was observed in AR3. This falls in the region between 2,550 and 2,770 cm^{-1}, which has recently been associated with a postulated hydrogen bonded network of three water molecules in the BR cytoplasmic channel that are involved in transport of a proton between Asp96 and the Schiff base [17]. In addition, the negative absorbance extending below 2,500 cm^{-1} to at least 1,800 cm^{-1} in BR has been assigned to a Zundel cation ($H_2O_5^+$) postulated to be part of the proton release group on the extracellular portion of the protein [18].

Note that most of the bands in the region below 3,500 cm^{-1} are unlikely to arise from individual water hydroxyl groups since they do not appear to shift significantly (e.g., >10 cm^{-1}) for AR3 in H_2O^{18} relative to H_2O (see Fig. 5). However, many of these bands were very broad and, due to high noise in the region, especially between 3,200 and 3,500 cm^{-1}, we cannot exclude possible shifts of order 10 cm^{-1}. Indeed, a number of OH vibrations have been assigned in BR in the region below 3,600 cm^{-1}, including bands at 3,607 and 3,577 cm^{-1} (−), which appeared during formation of the L intermediate [48].

5 Discussion and conclusions

The role of water molecules and possible Grotthuss-type proton transport chains in proton transporting membrane proteins such as BR and cytochrome oxidase has been an area of significant interest [19, 52–55]. The discovery of internal water molecules, which undergo structural changes during the BR photocycle, was initially based on low-temperature FTIR difference spectroscopy [7–9]. This approach, combined with site-directed mutagenesis, provided information about the approximate location of these waters in the BR structure [9, 48, 56, 57]. For example, disappearance of the 3,642 cm^{-1} band due to mutations in the active site led to the prediction that one or more waters are located near the Schiff base region of the protein [49, 58]. Similar assignments were also made for waters located in the cytoplasmic channel and at the proton release complex [48, 57].

X-ray diffraction studies provided definitive evidence for internal BR waters. One water molecule, designated W402, bridges between Asp85, Asp212, and the Schiff base (see Fig. 6). This water and two others (W401 and W406), along with negatively charged Asp85 and Asp212, form a pentagonal cluster and also interact with the SB (positive charge) and Arg82 (positive charge) to produce a charge-neutral quadropole complex similar to the structure first predicted on the basis of FTIR/site-directed mutagenesis studies [59]. Additional X-ray studies of BR photointermediates [60] indicate that, during M formation, this structure is disrupted by a proton transfer from the SB to Asp85, causing a small movement of Arg82 towards the extracellular domain and ultimately ejection of a proton as originally predicted [59]. A proton release complex is also involved in proton ejection. This is postulated to consist of two negatively charged residues, Glu194 and Glu204, and a positively charged water complex located near the extracellular medium [18, 61]. Several other water molecules are detected by X-ray diffraction located near the cytoplasmic portion

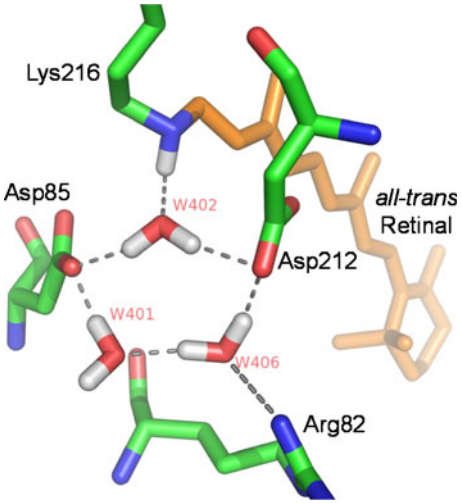

Fig. 6 X-ray crystallographic structure of BR from PDB coordinates 13CW [62] showing position of water molecules oriented as shown in Fig. 2 of [67]

of BR (e.g., W501 and 502) in the BR light-adapted state, which may form a proton transporting chain of waters during N formation [62–65].

The current study on AR3 reveals many similar features, including similar protein conformational changes during the photocycle and very similar retinal configurational changes based on the appearance of bands assigned to retinal vibrations for the light-adapted ground state as well as the K, M, and N intermediates. However, differences appear in the region above 3,600 cm^{-1} assigned to weakly hydrogen bonded internal water including a shift of the 3,642 cm^{-1} band in the primary phototransition. In BR, this band has been associated with W401 since its hydroxyl group does not appear to form a strong hydrogen bond, consistent with the high frequency of the band [19, 63, 66]. In further support of this assignment, combined quantum mechanical and molecular mechanical (QM/MM) calculations predict that W401 produces bands in the high-frequency range (unbounded hydroxyl) as well as at much lower frequency [67]. However, polarized FTIR measurements on this band are not consistent with the X-ray derived model, which indicates that the hydroxyl bond is parallel to the membrane normal compared to 60° [68]. The upshift in frequency we observe in AR3 compared to BR of this negative band indicates that if the pentagonal arrangement of waters seen in BR (Fig. 6) still exists in AR3, the comparable W401 is likely to be in a somewhat different environment that results in a weaker hydrogen bonding in the light-adapted state but not necessarily in the K intermediate. This is supported by the crystallographic structure of AR2 [13], where three water molecules still form a pentagonal cluster along with Asp85 and Asp212 but have altered positions and most likely different hydrogen bond strengths. Note also that Arg82 is not in a position to interact as strongly with W406 (see Fig. 6). A similar comparison cannot yet be made with AR3 until its structure is determined at high resolution.

The absence of bands at 3,670 and 3,655 cm^{-1} in the AR3→M, N difference spectra indicate that there may also be differences in the Schiff base reprotonation mechanism between BR and AR3. In support of this possibility, a recent detailed model for the BR SB reprotonation mechanism in BR postulates the existence of a chain of three hydrogen bonded water molecules, which spans the normally hydrophobic region between Asp96 and the Schiff base and could act as a Grotthuss-type proton transfer chain [17]. Besides giving

rise to IR bands appearing between 2,750 and 2,540 cm^{-1} during the M→N step in the photocycle [17] (see below), these high-frequency bands are assigned to two of the three water molecules in the chain designated as 501a and 501b. Our evidence clearly indicates that, if such a reprotonation chain of water molecules does exist in AR3, it does not give rise to such high-frequency bands associated with weakly hydrogen bonded waters.

In contrast, there is a strikingly high degree of similarity between the BR and AR3 FTIR difference spectrum below 3,600 cm^{-1}. This is particularly true for the broad IR continuum bands appearing in the region below 3,000 cm^{-1}, which have previously been assigned to networks of strongly hydrogen bonded waters. For example, a broad IR continuum absorbance below 2,500 cm^{-1} and extending to at least 1,800 cm^{-1} has been observed in BR during M formation [18] (below this it is difficult to observe such bands due to interference with protein and chromophore difference bands). This IR continuum agrees remarkably well with that predicted for a Zundel cation ($H_2O_5^+$) and has been associated on the basis of site-directed mutagenesis with a proton release complex formed between water molecules located near Glu204 and Glu194 [18]. The appearance of a similar negative absorbance change in AR3 (Fig. 5) indicates the existence of a similar mechanism for proton release.

Another example is the broad positive band appearing at 2,570 cm^{-1} in the M and N differences in both AR3 and BR (see Fig. 5). This is in agreement with earlier time-resolved FTIR measurements which find positive absorbance changes appearing during N formation between 2,550 and 2,770 cm^{-1} and assigned to the chain of three hydrogen bonded waters proposed to reprotonate the Schiff base during N formation [17].

Overall, our results indicate that AR3 and BR have a similar light-induced proton pumping mechanism. This is not surprising since almost all major residues that are considered to play a role in the BR pump mechanism are conserved in AR3. Nonetheless, our results point to specific differences in bands assigned to weakly hydrogen bonded water molecules, especially those previously assigned to specific waters seen in the BR crystallographic structure. However, water molecules which give rise to broad IR absorbance changes previously attributed to networks of strongly hydrogen bonded waters appear to be conserved in AR3. Further studies combining site-directed mutagenesis, isotope labeling, and time-resolved FTIR difference spectroscopy are now underway to further investigate possible differences and similarities in the BR and AR3 proton pumps.

Acknowledgements We thank David Oh for assistance of preparation in all AR3 samples, Dr. Edward Boyden (MIT) for providing a lentiviral backbone plasmid encoding Arch-EGFP (FCK:Arch-EGFP), and Drs. Xue Han at Boston University and Adam Cohen at Harvard University for helpful discussions.

References

1. Ihara, K., Umemura, T., Katagiri, I., Kitajima-Ihara, T., Sugiyama, Y., Kimura, Y., Mukohata, Y.: Evolution of the archaeal rhodopsins: evolution rate changes by gene duplication and functional differentiation. J. Mol. Biol. **285**, 163–174 (1999)
2. Stoeckenius, W.: The purple membrane of salt-loving bacteria. Sci. Am. **234**(6), 38–46 (1976)
3. Lanyi, J. K. : X-ray diffraction of bacteriorhodopsin photocycle intermediates. Mol. Membr. Biol. **21**, 143–150 (2004)
4. Rothschild, K.J.: FTIR difference spectroscopy of bacteriorhodopsin: toward a molecular model. J. Bioenerg. Biomembr. **24**, 147–167 (1992)
5. Lanyi, J.K.: Bacteriorhodopsin. Annu. Rev. Physiol. **66**, 665–688 (2004)
6. Xiao, Y., Hutson, M.S., Belenky, M., Herzfeld, J., Braiman, M.S.: Role of arginine-82 in fast proton release during the bacteriorhodopsin photocycle: a time-resolved FT-IR study of purple membranes containing 15N-labeled arginine. Biochemistry **43**, 12809–12818 (2004)

7. Maeda, A., Sasaki, J., Shichida, Y., Yoshizawa, T.: Water structural changes in the bacteriorhodopsin photocycle: analysis by Fourier-transform infrared spectroscopy. J. Biochem. **31**, 462–467 (1992)
8. Fischer, W.B., Rothschild, K.J.: Water molecules are active during the primary photoreaction of bacteriorhodopsin. Proc. SPIE **2089**, 118 (1993)
9. Fischer, W., Sonar, S., Marti, T., Khorana, H.G., Rothschild, K.J.: Detection of a water molecule in the active site of bacteriorhodopsin: hydrogen bonding changes during the primary photoreaction. Biochemistry **33**, 12757–12762 (1994)
10. Weinwurm, M., Dellago, C.: Vibrational spectroscopy of water in narrow nanopores. J. Phys. Chem. B **115**, 5268–5277 (2011)
11. Bellamy, L.J.: The Infrared Spectra of Complex Molecules. Chapman and Hall, London (1968)
12. Zundel, G.: Hydrogen-bonded chains with large proton polarizability as charge conductors in proteins Bacteriorhodopsin and the F subunit of *E. coli.* J. Mol. Struct. **322**, 33–42 (1994)
13. Enami, N., Yoshimura, K., Murakami, M., Okumura, H., Ihara, K., Kouyama, T.: Crystal structures of archaerhodopsin-1 and -2: common structural motif in archaeal light-driven proton pumps. J. Mol. Biol. **358**, 675–685 (2006)
14. Chow, B.Y., Han, X., Dobry, A.S., Qian, X., Chuong, A.S., Li, M., Henninger, M.A., Belfort, G.M., Lin, Y., Monahan, P.E., Boyden, E.S.: High-performance genetically targetable optical neural silencing by light-driven proton pumps. Nature **463**, 98–102 (2010)
15. Kralj, J.M., Douglass, A.D., Hochbaum, D.R., McLaurin, D., Cohen, A.E.: Optical recording of action potentials in mammalian neurons using a microbial rhodopsin. Nat. Methods (in press)
16. Deisseroth, K.: Optogenetics. Nat. Methods **8**, 26–29 (2011)
17. Freier, E., Wolf, S., Gerwert, K.: Proton transfer via a transient linear water-molecule chain in a membrane protein. Proc. Natl. Acad. Sci. U.S.A. **108**, 11435–11439 (2011)
18. Garczarek, F., Brown, L.S., Lanyi, J.K., Gerwert, K.: Proton binding within a membrane protein by a protonated water cluster. Proc. Natl. Acad. Sci. U.S.A. **102**, 3633–3638 (2005)
19. Garczarek, F., Gerwert, K.: Functional waters in intraprotein proton transfer monitored by FTIR difference spectroscopy. Nature **439**, 109–112 (2006)
20. Bergo, V., Spudich, E.N., Spudich, J.L., Rothschild, K.J.: Conformational changes detected in a sensory rhodopsin II-transducer complex. J. Biol. Chem. **278**, 36556–36562 (2003)
21. Bergo, V., Amsden, J.J., Spudich, E.N., Spudich, J.L., Rothschild, K.J.: Structural changes in the photoactive site of proteorhodopsin during the primary photoreaction. Biochemistry **43**, 9075–9083 (2004)
22. Kralj, J.M., Bergo, V.B., Amsden, J.J., Spudich, E.N., Spudich, J.L., Rothschild, K.J.: Protonation state of Glu142 differs in the green- and blue-absorbing variants of proteorhodopsin. Biochemistry **47**, 3447–3453 (2008)
23. Ikeda, D., Furutani, Y., Kandori, H.: FTIR study of the retinal Schiff base and internal water molecules of proteorhodopsin. Biochemistry **46**, 5365–5373 (2007)
24. Rothschild, K., Marrero, H.: Infrared evidence that the Schiff base of bacteriorhodopsin is protonated: bR570 and K intermediates. Proc. Natl. Acad. Sci. U.S.A. **79**, 4045–4049 (1982)
25. Siebert, F., Maentele, W.: Investigation of the primary photochemistry of bacteriorhodopsin by low-temperature Fourier-transform infrared spectroscopy. Eur. J. Biochem. **130**, 565–573 (1983)
26. Bergo, V., Spudich, E.N., Spudich, J.L., Rothschild, K.J.: A Fourier-transform infrared study of Neurospora rhodopsin: similarities with archaeal rhodopsins. Photochem. Photobiol. **76**, 341–349 (2002)
27. Kandori, H., Furutani, Y., Shimono, K., Shichida, Y., Kamo, N.: Internal water molecules of pharaonis phoborhodopsin studied by low-temperature infrared spectroscopy. Biochemistry **40**, 15693–15698 (2001)
28. Roepe, P., Scherrer, P., Ahl, P.L., Das Gupta, S.K., Bogomolni, R.A., Herzfeld, J., Rothschild, K.J.: Tyrosine and carboxyl protonation changes in the bacteriorhodopsin photocycle. 2. Tyrosines-26 and -64. Biochemistry **26**, 6708–6717 (1987)
29. Bergo, V.B., Ntefidou, M., Trivedi, V.D., Amsden, J.J., Kralj, J.M., Rothschild, K.J., Spudich, J.L.: Conformational changes in the photocycle of Anabaena sensory rhodopsin: absence of the Schiff base counterion protonation signal. J. Biol. Chem. **281**, 15208–15214 (2006)
30. Amsden, J.J., Kralj, J.M., Bergo, V.B., Spudich, E.N., Spudich, J.L., Rothschild, K.J.: Different structural changes occur in blue- and green-proteorhodopsins during the primary photoreaction. Biochemistry **47**, 11490–11498 (2008)
31. Bagley, K., Dollinger, G., Eisenstein, L., Singh, A.K., Zimanyi, L.: Fourier-transform infrared difference spectroscopy of bacteriorhodopsin and its photoproducts. Proc. Natl. Acad. Sci. U.S.A. **79**, 4972–4976 (1982)

32. Rothschild, K.J., Marrero, H., Braiman, M., Mathies, R.: Primary photochemistry of bacteriorhodopsin: comparison of Fourier-transform infrared difference spectra with resonance Raman spectra. Photochem. Photobiol. **40**, 675–679 (1984)
33. Aton, B., Doukas, A.G., Callender, R.H., Becher, B., Ebrey, T.G.: Resonance Raman studies of the purple membrane. Biochemistry **16**, 2995–2999 (1977)
34. Bergo, V., Mamaev, S., Olejnik, J., Rothschild, K.J.: Methionine changes in bacteriorhodopsin detected by FTIR and cell-free selenomethionine substitution. Biophys. J. **84**, 960–966 (2003)
35. Rothschild, K.J., Roepe, P., Gillespie, J.: Fourier-transform infrared spectroscopic evidence for the existence of two conformations of the bacteriorhodopsin primary photoproduct at low temperature. Biochim. Biophys. Acta. **808**, 140–148 (1985)
36. Dioumaev, A.K., Lanyi, J.K.: Bacteriorhodopsin photocycle at cryogenic temperatures reveals distributed barriers of conformational substates. Proc. Natl. Acad. Sci. U.S.A. **104**, 9621–9626 (2007)
37. Smith, S.O., Braiman, M.S., Myers, A.B., Pardoen, J.A., Courtin, J.M.L., Winkel, C., Lugtenburg, J., Mathies, R.A.: Vibrational analysis of the all-trans-retinal chromophore in light-adapted bacteriorhodopsin. J. Am. Chem. Soc. **109**, 3108–3125 (1987)
38. Smith, S.O., Pardoen, J.A., Lugtenburg, J., Mathies, R.A.: Vibrational analysis of the 13-cis-retinal chromophore in dark-adapted bacteriorhodopsin. J. Phys. Chem. **91**, 804–819 (1987)
39. Kralj, J.M., Bergo, V.B., Amsden, J.J., Spudich, E.N., Spudich, J.L., Rothschild, K.J.: Protonation state of Glu142 differs in the green- and blue-absorbing variants of proteorhodopsin. Biochemistry **47**, 3447–3453 (2008)
40. Dioumaev, A.K., Brown, L.S., Shih, J., Spudich, E.N., Spudich, J.L., Lanyi, J.K.: Proton transfers in the photochemical reaction cycle of proteorhodopsin. Biochemistry **41**, 5348–5358 (2002)
41. Braiman, M.S., Mogi, T., Stern, L.J., Hackett, N.R., Chao, B.H., Khorana, H.G., Rothschild, K.J.: Vibrational spectroscopy of bacteriorhodopsin mutants: I. Tyrosine-185 protonates and deprotonates during the photocycle. Proteins **3**, 219–229 (1988)
42. Bousché, O., Braiman, M., He, Y.W., Marti, T., Khorana, H.G., Rothschild, K.J.: Vibrational spectroscopy of bacteriorhodopsin mutants. Evidence that ASP-96 deprotonates during the M–N transition. J. Biol. Chem. **266**, 11063–11067 (1991)
43. Bousche, O., Sonar, S., Krebs, M.P., Khorana, H.G., Rothschild, K.J.: Time-resolved Fourier-transform infrared spectroscopy of the bacteriorhodopsin mutant Tyr-185→Phe: Asp-96 reprotonates during O formation; Asp-85 and Asp-212 deprotonate during O decay. Photochem. Photobiol. **56**, 1085–1095 (1992)
44. Braiman, M.S., Bousché, O., Rothschild, K.J.: Protein dynamics in the bacteriorhodopsin photocycle: submillisecond Fourier-transform infrared spectra of the L, M, and N photointermediates. Proc. Natl. Acad. Sci. U.S.A. **88**, 2388–2392 (1991)
45. Roepe, P., Ahl, P.L., Das Gupta, S.K., Herzfeld, J., Rothschild, K.J.: Tyrosine and carboxyl protonation changes in the bacteriorhodopsin photocycle. 1. M412 and L550 intermediates. Biochemistry **26**, 6696–6707 (1987)
46. Braiman, M.S., Mogi, T., Marti, T., Stern, L.J., Khorana, H.G., Rothschild, K.J.: Vibrational spectroscopy of bacteriorhodopsin mutants: light-driven proton transport involves protonation changes of aspartic acid residues 85, 96, and 212. Biochemistry **27**, 8516–8520 (1988)
47. Kates, M., Kushwaha, S.C., Sprott, G.D. (eds.): Lipids of Purple Membrane from Extreme Halophiles and of Methanogenic Bacteria. Academic Press, New York (1982)
48. Kandori, H.: Role of internal water molecules in bacteriorhodopsin. Biochim. Biophys. Acta **1460**, 177–191 (2000)
49. Fischer, W.B., Sonar, S., Marti, T., Khorana, H.G., Rothschild, K.J.: Detection of a water molecule in the active-site of bacteriorhodopsin: hydrogen bonding changes during the primary photoreaction. Biochemistry **33**, 12757–12762 (1994)
50. Maeda, A., Sasaki, J., Ohkita, Y.J., Simpson, M., Herzfeld, J.: Tryptophan perturbation in the L intermediate of bacteriorhodopsin: Fourier transform infrared analysis with indole-15N shift. Biochemistry **31**, 12543–12545 (1992)
51. Liu, X., Lee, M.J., Coleman, M., Rath, P., Nilsson, A., Fischer, W.B., Bizounok, M., Herzfeld, J., Karstens, W.F., Raap, J., Lugtenburg, J., Rothschild, K.J.: Detection of threonine structural changes upon formation of the M- intermediate of bacteriorhodopsin: evidence for assignment to Thr-89. Biochim. Biophys. Acta **1365**, 363–372 (1998)
52. Tuckerman, M.E., Chandra, A., Marx, D.: Structure and dynamics of OH-(aq). Acc. Chem. Res. **39**, 151–158 (2006)
53. Mathias, G., Marx, D.: Structures and spectral signatures of protonated water networks in bacteriorhodopsin. Proc. Natl. Acad. Sci. U.S.A. **104**, 6980–6985 (2007)

54. Ferreira, K.N., Iverson, T.M., Maghlaoui, K., Barber, J., Iwata, S.: Architecture of the photosynthetic oxygen-evolving center. Science **303**, 1831–1838 (2004)
55. Belevich, I., Verkhovsky, M.I., Wikstrom, M.: Proton-coupled electron transfer drives the proton pump of cytochrome c oxidase. Nature **440**, 829–832 (2006)
56. Maeda, A., Kandori, H., Yamazaki, Y., Nishimura, S., Hatanaka, M., Chon, Y.S., Sasaki, J., Needleman, R., Lanyi, J.K.: Intramembrane signaling mediated by hydrogen-bonding of water and carboxyl groups in bacteriorhodopsin and rhodopsin. J. Biochem. **121**, 399–406 (1997)
57. Maeda, A., Tomson, F.L., Gennis, R.B., Kandori, H., Ebrey, T.G., Balashov, S.P.: Relocation of internal bound water in bacteriorhodopsin during the photoreaction of M at low temperatures: an FTIR study. Biochemistry **39**, 10154–10162 (2000)
58. Maeda, A., Sasaki, J., Yamazaki, Y., Needleman, R., Lanyi, J.K.: Interaction of aspartate-85 with a water molecule and the protonated Schiff base in the L intermediate of bacteriorhodopsin: a Fourier-transform infrared spectroscopic study. Biochemistry **33**, 1713–1717 (1994)
59. Braiman, M.S., Mogi, T., Marti, T., Stern, L.J., Khorana, H.G., Rothschild, K.J.: Vibrational spectroscopy of bacteriorhodopsin mutants: light-driven proton transport involves protonation changes of aspartic acid residues 85, 96, and 212. Biochemistry **27**, 8516–8520 (1988)
60. Lanyi, J., Schobert, B.: Crystallographic structure of the retinal and the protein after deprotonation of the Schiff base: the switch in the bacteriorhodopsin photocycle. J. Mol. Biol. **321**, 727–737 (2002)
61. Brown, L.S., Sasaki, J., Kandori, H., Maeda, A., Needleman, R., Lanyi, J.K.: Glutamic acid 204 is the terminal proton release group at the extracellular surface of bacteriorhodopsin. J. Biol. Chem. **270**, 27122–27126 (1995)
62. Luecke, H., Schobert, B., Richter, H.T., Cartailler, J.P., Lanyi, J.K.: Structure of bacteriorhodopsin at 1.55 Å resolution. J. Mol. Biol. **291**, 899–911 (1999)
63. Luecke, H., Schobert, B., Richter, H.T., Cartailler, J.P., Lanyi, J.K.: Structural changes in bacteriorhodopsin during ion transport at 2 angstrom resolution. Science **286**, 255–261 (1999)
64. Schobert, B., Brown, L.S., Lanyi, J.K.: Crystallographic structures of the M and N intermediates of bacteriorhodopsin: assembly of a hydrogen-bonded chain of water molecules between Asp-96 and the retinal Schiff base. J. Mol. Biol. **330**, 553–570 (2003)
65. Lanyi, J.K., Schobert, B.: Mechanism of proton transport in bacteriorhodopsin from crystallographic structures of the K, L, M1, M2, and M2′ intermediates of the photocycle. J. Mol. Biol. **328**, 439–450 (2003)
66. Shibata, M., Kandori, H.: FTIR studies of internal water molecules in the Schiff base region of bacteriorhodopsin. Biochemistry **44**, 7406–7413 (2005)
67. Baer, M., Mathias, G., Kuo, I.F., Tobias, D.J., Mundy, C.J., Marx, D.: Spectral signatures of the pentagonal water cluster in bacteriorhodopsin. Chemphyschem. **9**, 2703–2707 (2008)
68. Hatanaka, M., Kandori, H., Maeda, A.: Localization and orientation of functional water molecules in bacteriorhodopsin as revealed by polarized Fourier-transform infrared spectroscopy. Biophys. J. **73**, 1001–1006 (1997)